Electrocatalyst Screening on a Massive Array of Closed Bipolar Microelectrodes

Todd J. Anderson, Peter A. Defnet, Robin A. Cheung, and Bo Zhang*
Department of Chemistry, University of Washington Seattle Washington 98195 United States

Corresponding author, zhangb@uw.edu

Abstract. Herein, we report the use of a massive array of bipolar ultramicroelectrodes (UMEs) in conjunction with electrochemiluminescence (ECL) imaging as a novel electroanalytical platform for rapid screening of electrocatalysts. Following our recent work on carbon bipolar UME arrays, we have developed asymmetric carbon-gold bipolar UME arrays where each carbon UME is coated by a thin gold film on one side. To generate large quantities of compositionally varied electrocatalyst samples, a radial gradient of catalytic metal is electrodeposited on the surface of these UME arrays by delivering a plume of metal salt solution to the array surface with a micropipette while the entire array is biased at a reducing potential. We then utilize these bipolar UME arrays to investigate the impact of varied $Ni(OH)_2$ coverage on the catalytic activity for hydrogen evolution reaction (HER) of an Au surface in alkaline solution, with the catalytic performance of the modified Au being confirmed to exhibit a peak-shaped dependence on increasing $Ni(OH)_2$ coverage. Our future work will expand this unique platform to enable the screening of various metal alloys by incorporating additional micropipettes for delivering multiple metal salts to the array during the gradient electrodeposition process.

Introduction

Given the large number of properties which influence electrocatalytic performance (*e.g.,* particle morphology,[1] surface ligands,[2] alloy composition,[3] atomic ordering,[4] etc.), high-throughput screening methods are critical to inform the discovery and optimization of new electrocatalysts. Such screening is typically carried out via a combinatorial approach in which compositionally stepped or gradient samples are synthesized and subsequently screened to ascertain the effects of selected physical properties on the catalytic activity toward a reaction of interest.[5–7] Because the efficiency of such a scheme is partially governed by the sample creation time, this step has been targeted for improvement in various studies. Distribution of catalyst-bearing conductive inks in an arrayed pattern to enable screening of various composites is perhaps the simplest sample preparation method[8,9]; mixtures of metal salt solutions may also be dispensed in a similar manner followed by chemical or electrochemical treatment to form catalytic alloy spots of the desired metals.[10–12] However, while both of these techniques have been automated using inkjet printing,[13] a piezodispensing apparatus,[14] or a scanning flow cell,[15] the sequential nature of such an approach greatly increases the time required for the creation of large sample libraries. Several forms of physical vapor deposition (PVD) have been employed to generate well-controlled gradients of electrocatalytic metals via co-deposition from multiple sources.[16–20] This approach is particularly attractive due to the extremely large number of alloy compositions which may be created in a single deposition, but the expense of the requisite instrumentation and metal sources renders it cost-prohibitive for many applications. Exploitation of the potential gradient along an open bipolar electrode to manipulate the electrodeposition rates of multiple metals has also been proposed,[21] although the combinations of metals and achievable gradients are somewhat constrained by difference in redox potentials of the deposited species.

Several strategies have also been employed to maximize the throughput of electrocatalyst activity detection. Scanning techniques in which an ultramicroelectrode (UME),[11,12,14,17,22–26] reference/counter electrode couple,[27,28] optical fiber, flow cell,[29,30] or laser[31] is rastered across a catalytic surface while the current response is recorded have been extensively utilized to map the catalytic activity of

compositionally varied samples, but the experiment time is typically quite long due to the use of a single probe. Individually addressable electrode arrays offer an improvement in screening parallelization,[8,9,13,18,32–35] but are limited in size due to the number of data channels which must be simultaneously monitored; additionally, fabrication of such devices is extremely challenging due to the large number of connecting leads. Optical imaging of reaction products originating from an electrocatalyst array via a pH-dependent fluorescent reporter,[10,17,32] photochromic film,[36,37] or gas bubble detection[38] provides a more rapid, albeit indirect, approach to monitoring catalytic activity, but free diffusion of the detected species limits the capacity of these techniques to screen compositional gradients.

Open bipolar electrodes (BPEs) address the majority of these shortcomings by allowing a reaction of interest to be coupled to a complementary reporter reaction via the application of an external polarizing potential, thereby providing a direct measure of catalytic activity without necessitating that electrical contact be maintained with the electrode.[19,21,39–41] When coupled with a luminescent reporter reaction such as electrochemiluminescence (ECL), this scheme yields an optical signal which is directly proportional to the catalytic current and easily scalable for many BPEs arranged in parallel.[42–44] Unfortunately, the presence of a competing ionic current pathway in open bipolar systems necessitates the use of relatively large electrodes to yield a sufficient potential difference across the electrode surface to induce coupling,[45,46] thereby limiting the maximum array density and number of catalyst compositions which may be simultaneously screened. Closed BPE arrays do not possess such a parallel ionic current pathway due to segregation of the detecting and reporting solutions on opposite sides of the array, meaning that the majority of the applied potential drop occurs at the electrode solution/interface when solution resistance is low as a result of high supporting electrolyte concentration.[47,48]; hence, electrode size does not affect functionality. However, despite the absence of any constraints to array size and resolution, all of the electrocatalytic screening studies utilizing closed BPE arrays which have been carried out at the time of this writing are limited to small arrays comprised of only a handful of electrodes.[49,50]

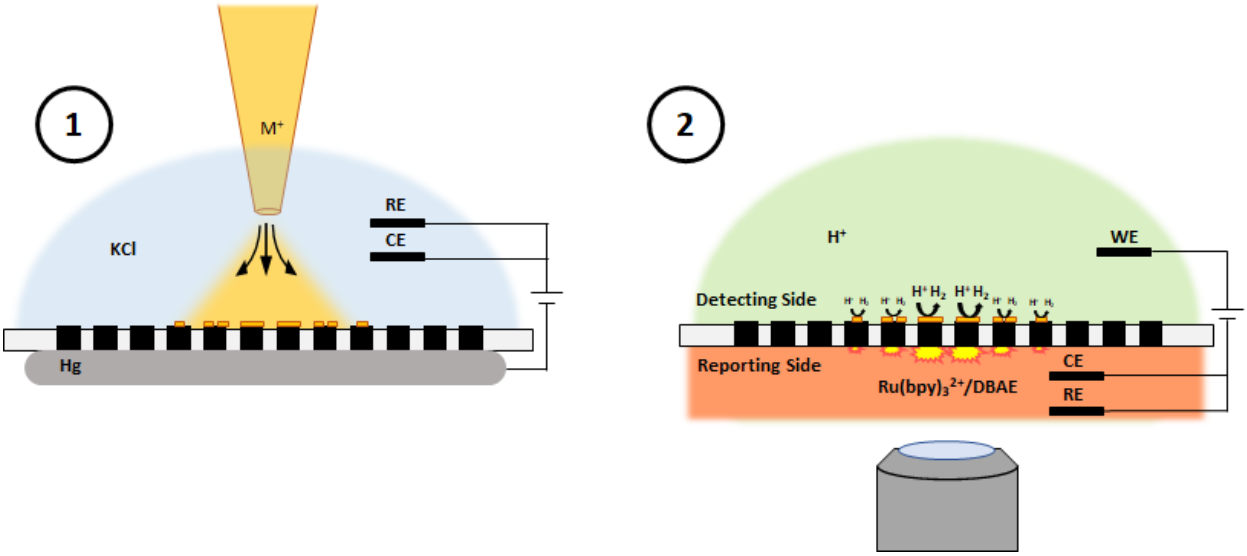

Scheme 1. Diagram of gradient electrodeposition process (step 1) and highly parallelized HER electrocatalyst screening via coupling to ECL using a BPE array (step 2).

We therefore present a highly parallelized electrocatalyst screening platform based on ECL imaging with massive microfabricated closed bipolar UME arrays which we have reported in a previous publication.[51] The excellent uniformity of electrochemical response which was demonstrated for these devices in this prior work indicates that they are well-suited to comparative studies of electrocatalyst candidates coated on different electrodes. By imaging a subset consisting of only 4% of the surface area of one of these arrays, we are able to map the onset potentials of electrocatalytic materials deposited on over 6000 separate electrodes; this degree of screening parallelization is over an order of magnitude greater than the largest array-based electrocatalyst screening study reported in the literature.[18] Additionally, we introduce a facile method for selective electrodeposition of catalytic metals on the array surface by establishing direct electrical contact with all of the electrodes in the array using a Hg drop biased at a reducing potential. This electrodeposition scheme is much more straightforward than existing techniques for modifying BPE arrays via electrodeposition which rely on coupling metal salt reduction to a mediating oxidation reaction[50,52] and can be further extended to enable screening of a gradient in the deposited metal composition by delivering metal salt solution to the array surface via a micropipette.

Lastly, we present an alternate fabrication scheme for our closed bipolar UME arrays which incorporates an Au coating of the constituent electrodes. These Au-modified arrays are used in conjunction with the aforementioned gradient electrodeposition technique to demonstrate the utility of this platform by investigating the heterogeneity in activity of a compositionally varied metal/metal hydroxide HER electrocatalyst.

Experimental Section

Chemicals and Materials. The following chemicals were used as received from their manufacturers: nitric acid (HNO_3, Sigma-Aldrich, 70%), perchloric acid ($HClO_4$, Sigma-Aldrich, 70%), hydrochloric acid (HCl, Sigma-Aldrich, 37%), sodium perchlorate monohydrate ($NaClO_4 \cdot H_2O$, Fluka, >99%), potassium chloride (KCl, Fluka, >99%), potassium hydroxide (KOH, Sigma-Aldrich, 99.99%), platinum(IV) chloride ($PtCl_4$, Sigma-Aldrich, >99.9%), nickel(II) chloride ($NiCl_2$, Sigma-Aldrich, 98%), sodium chloride (NaCl, Sigma-Aldrich, >99%), gold(III) chloride ($AuCl_3$, Salt Lake Metals, 1.534% solution), Gold Etch TFA (Transene), tris(2,2'-bipyridyl)dichlororuthenium(II) hexahydrate ($Ru(bpy)_3Cl_2 \cdot 6H_2O$, Sigma-Aldrich, 99.5%), 2-(dibutylamino)ethanol (DBAE, Sigma-Aldrich, 99%), potassium phosphate monobasic (KH_2PO_4, J.T. Baker, 99.9%), potassium phosphate dibasic (K_2HPO_4, J.T. Baker, 99.9%). All solutions were prepared with 18.2 MΩ·cm deionized water from a Barnstead NANOpure water purification system (Thermo Scientific).

Array Fabrication. Bipolar carbon UME arrays were fabricated and prepared for imaging using the same procedure described in our previous publication.[51] Au-modified arrays were fabricated using a similar procedure. However, a 200 nm Au film was first deposited onto the array surface using a sputter coater (Evatec) prior to insulation with Parylene C. Additionally, annealing was carried out after exposure of the electrodes via dry etching to prevent premature delamination of the arrays from the Si substrates.

Array Modification via Electrodeposition. Potential was controlled for all electrodeposition processes using an EG&G Princeton Applied Research Model 273A Potentiostat/Galvanostat. The Hg drop was contained on a modified microscope slide using an o-ring which was held in place with epoxy.

Electrical contact was made with the Hg drop using two bundles of carbon fibers positioned on each side of the o-ring. A commercial reference electrode (BASi) and a Pt foil counter electrode were used to form an electrochemical cell over the surface of the array. Au electrodeposition was performed with 50 mM $AuCl_3$ solution at 1.5 mA for 2 min using an array half-covered with polydimethylsiloxane (PDMS). Metal salt solutions for gradient electrodeposition were delivered from a z-height of 100 μm above the array surface using a 5 μm diameter pulled quartz micropipette in conjunction with an Eppendorf Femtojet at a pressure of 0.22 PSI for 100 s. An Olympus CK40 inverted microscope and electronic micromanipulator (Sutter) were used to position the pipette prior to injection. All gradient electrodepositions were carried out in a 100 mM KCl supporting electrolyte solution. Pt deposition was performed by injection of 50 mM $PtCl_4$ solution at -0.1 V vs. Ag/AgCl; $Ni(OH)_2$ deposition was performed by injection of 1 M $NiCl_2$ 100 mM NaCl pH 3.6 solution at -1 V vs. Ag/AgCl followed by cycling from 0.1 to 0.5 V vs. Ag/AgCl at 5 mV/s in 100 mM KOH for 25 cycles.

Imaging of Electrocatalytic Activity. Potential was driven across the array using an EG&G Princeton Applied Research Model 175 universal programmer linked to a 3-electrode CV-27 potentiostat (BAS) with 3 Ag/AgCl electrodes. Reference and counter electrodes were placed in the bottom ECL solution and the working electrode was placed in the top solution. Wires were freshly chlorided prior to each experiment using a 1:1 solution of 70% HNO_3 and 3 M KCl. All imaging experiments were recorded on an Andor iXon 897E EMCCD camera cooled to -80 ºC with 30 ms exposure, 300 EM Gain, 5.1x pre-amplifier gain, 0.3 μs vertical pixel shift speed, and 10 MHz readout rate. Videos contained 1500 frames with 512×512 pixels. An Olympus IX70 microscope equipped with a 4x (0.1 NA Olympus Plan N) objective was used to image the array. Each pixel measured 3.92 μm, yielding a 4.0×10^6 μm^2 field of view and allowing ~6000 full electrodes in each frame. The ECL solution below the array was contained on the microscope stage using a home-built device fabricated from three 1.0 mm thick glass slides (VWR). One slide was used as the base and two were positioned laterally about 1 cm apart, creating a 1 mm deep channel for ECL solution containment. Epoxy was used to prevent solution leakage.

ECL voltammograms of the HER in acid were collected using a driving voltage sweep of 0 to 3 V vs. Ag/AgCl at 200 mV/s to couple the HER in 100 mM $HClO_4$ 100 mM NaCl above the array to anodic ECL in 25 mM $Ru(bpy)_3^{2+}$ 20 mM DBAE 100 mM phosphate buffer (PB) pH 7.4 below the array; alkaline HER ECL voltammograms were collected using a driving voltage sweep of 0 to 4 V vs. Ag/AgCl at 200 mV/s to couple HER in 100 mM KOH to the same anodic ECL solution. The camera and potentiostat were simultaneously triggered using a custom LabVIEW 2013 program and ECL intensity-potential (I_{ECL}-V) videos were collected using the conditions described above.

Analysis of ECL Video Data. ImageJ was used to designate each electrode as a separate region of interest (ROI) in the collected videos and extract the ECL intensity traces for all electrodes. These traces were then analyzed using a custom Python script which determined the frame number at which the ECL intensity first exceeded 180 counts and converted this value to an applied potential using the voltage scan rate. These potentials were then assigned color values and mapped to their corresponding ROIs to yield false color plots of the coupling onset potentials of the electrodes.

$Ni(OH)_2$ Modification of Au UME. The Au electrode was fabricated by sealing a piece of Au wire in a glass capillary[53] prior to characterization using cyclic voltammetry in 1 mM FcMeOH 100 mM KCl solution. Variable $Ni(OH)_2$ coverage was achieved by immersing the electrode in the aforementioned $NiCl_2$ solution for intervals ranging from 10 s to 5 min. Alkaline HER activity was evaluated by monitoring the current response of the UME in 100 mM KOH using a potential sweep of 0 to -2 V vs. Ag/AgCl at 200 mV/s. The electrode was polished after the collection of each voltammogram to regenerate the Au surface.

Results and Discussion

Modification of Bipolar UME Arrays via Electrodeposition. To facilitate electrodeposition of a catalytic metal on the detecting side of a carbon bipolar UME array, a Hg drop was used to make electrical contact with the reporting poles of all electrodes in the array which allowed the same potential

to be simultaneously applied across the array's entire electroactive surface and eliminated the need for bipolar coupling of the metal salt reduction to a separate oxidation mediator reaction. This approach also offers the benefit of enabling selective modification of subsets of the array by blocking off portions of the lower surface with thin sheets of polydimethylsiloxane (PDMS) before bringing it in contact with the Hg, thereby preventing electrodeposition from occurring in these regions. To carry out an electrodeposition, the well on the detecting side of an array was first filled with a metal salt solution, after which the opposite side was brought into contact with the Hg drop. An Ag/AgCl reference electrode and Pt foil counter electrode were then immersed in the solution to form an electrochemical cell in which the entire array served as the working electrode (see **Figure 1a**).

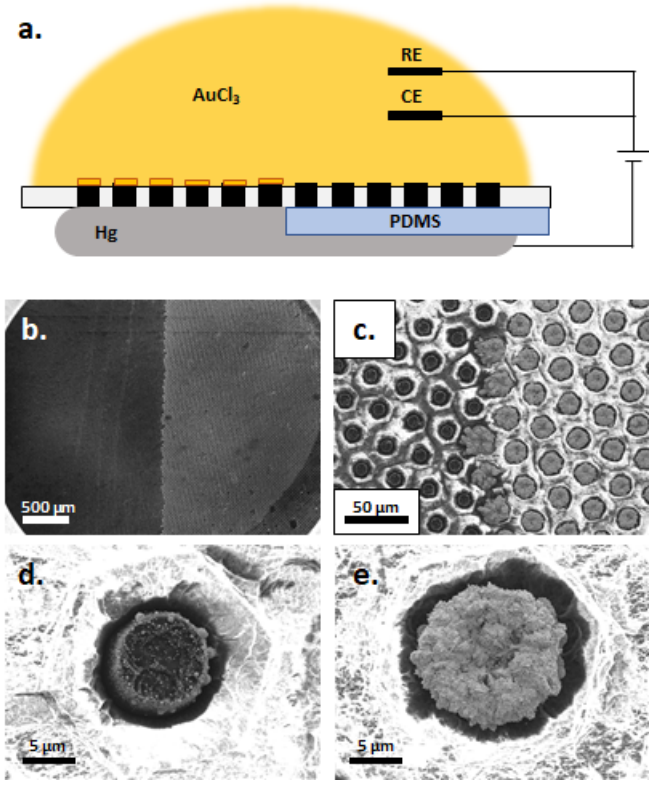

Figure 1. (a) Diagram of selective electrodeposition technique. (b) SEM image of an Au deposition which was carried out using 50 mM $AuCl_3$ for 2 min at 1.5 mA over half of a bipolar carbon UME array. (c) Zoomed SEM image of the boundary between the Au modified and unmodified regions of the same array. Representative images of (d) a bare carbon electrode and (e) an Au modified electrode.

Figure 1b shows an example of an array which was modified with Au in this manner across half of the surface via galvanostatic electrodeposition from a 50 mM solution of $AuCl_3$. The coverage of the

electrodes in the Au-modified portion of the array indicates both that electrical contact was made with all of the electrodes and that a consistent potential was applied across the surface. The Au overgrowth observed in **Figure 1b** at the border between the modified and unmodified portions of the array may be attributed to the higher Au ion concentration which existed along this boundary due to depletion of metal ions above the half of the array which experienced a potential bias. Note that the residue observed on the representative bare carbon electrode shown in **Figure 1c** may be attributed to salt deposits left behind after drying the array.

Gradient Electrodeposition of Electrocatalysts. Although the preceding selective electrodeposition method can be leveraged to enable comparative catalytic studies of the activity of various material compositions deposited sequentially across adjacent regions of a carbon bipolar UME array, such a process would be extremely time-consuming and does not take full advantage of the array's impressive resolution and imaging capacity. To introduce a radial gradient in the amount of catalytic metal deposited across an array, a method was devised in which a plume of metal salt solution was delivered to the biased array surface via a micropipette in a process similar in principle to other studies in which a redox species was "puffed" toward the surface of an electrode immersed in supporting electrolyte solution[51,54,55] (see step 1 of **Scheme 1**). First, the well on the detecting side of an array was filled with supporting electrolyte solution, after which the opposite side was brought into contact with the Hg drop and a reference electrode and Pt foil counter electrode were immersed in the electrolyte solution. Next, a 5 μm diameter micropipette filled with a metal salt solution was lowered through a hole in the counter electrode and held ~100 μm above the array surface. The Hg drop was then biased at a reducing potential and a pressure-injection module was used to dispense the metal salt solution at the surface of the array. Due to dilution of the pipette contents by the surrounding electrolyte solution after injection, a metal ion concentration gradient was formed about the pipette orifice over the course of the deposition.[56] **Figure 2f** shows an energy dispersive spectroscopy (EDS) map of the results of a Pt injection/deposition experiment with the corresponding scanning electron microscopy (SEM) image displayed in **Figure S1**. Note that there is a clear radial decrease in the amount of metal deposited on the electrodes about the injection site

with the tailing observed toward the upper portion of the image being due to positioning the pipette at a slight angle from normal to the array surface. Variability of this sort which may occur from one deposition experiment to another does not negatively impact the utility of the technique so long as a significant degree of variation exists across the entire electrocatalyst gradient such that a large number of electrocatalyst compositions are generated in a single experiment.

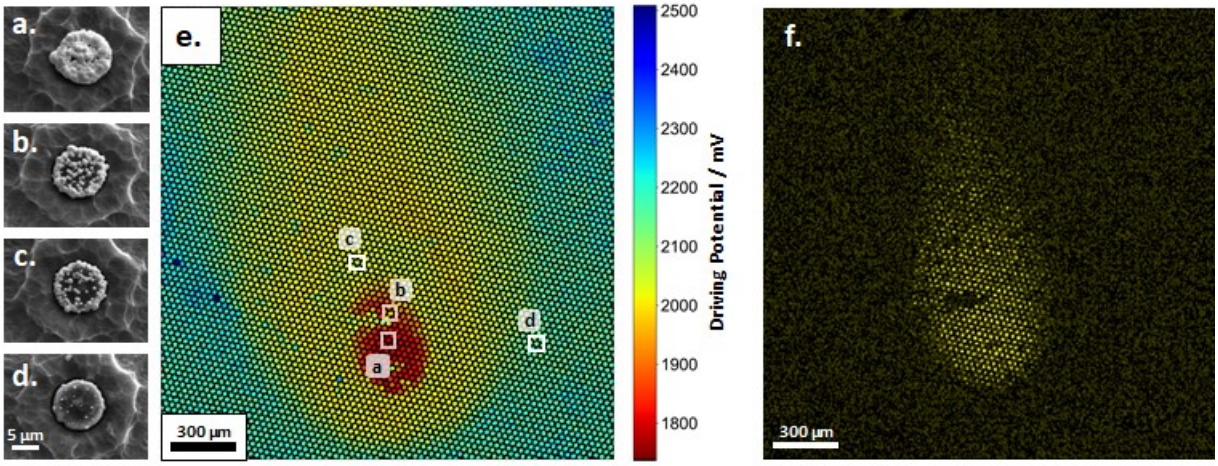

Figure 2. (a-d) SEM images of selected electrodes from the Pt gradient deposition site. (e) False color plot of HER onset driving potentials of the Pt gradient deposition site in 100 mM $HClO_4$ 100 mM NaCl coupled to anodic ECL with SEM-imaged electrodes labeled. (f) EDS map of Pt across gradient deposition site.

Electrocatalyst Screening via Bipolar Coupling to ECL. After modification of an array via this gradient electrodeposition technique, the activity of the Pt-modified electrodes toward the hydrogen evolution reaction (HER) was imaged via coupling to a $Ru(bpy)_3^{2+}$-based ECL system with the aim of demonstrating the applicability of this platform toward highly parallelized electrocatalyst screening (see step 2 of **Scheme 1**). The well on the detecting side of a metal-modified array was first filled with an acid solution, after which the reporting side was immersed in anodic ECL solution and the driving voltage across the array swept from 0 to 3 V; this applied potential induced coupling of the HER on one side of the array to anodic ECL on the other, the intensity of which was monitored and recorded as shown in **Movie S1** in which the ECL signal increases with the applied potential in a roughly linear fashion. Only a single scan was recorded since prolonged ECL generation on the electrode surfaces resulted in fouling

which negatively impacted the optical signal detected during subsequent scans. Note that the dark line observed at higher potentials is due to some sort of contamination deposited on the array surface.

Given that the current through an electrode of a bipolar array is directly related to the ECL intensity emanating from its reporting pole, the intensity vs. driving voltage trace (I_{ECL}-V) for each electrode could be used to determine the applied potential necessary to bring about the onset of HER. Mapping of HER onset driving voltage for all of the electrodes in an array was carried out using a custom Python script which extracted I_{ECL}-V traces for all ~6000 electrodes in the field-of-view and separately determined the driving potential necessary for each electrode to reach an ECL intensity threshold slightly above the noise level of the camera (180 counts). The coupling potential across a closed bipolar system is equal to the difference in formal potentials of the species involved in the two half reactions occurring on the poles (see Equation 1 below).

$$E_{coupling} = E^{\circ\prime}{}_{species\,1} - E^{\circ\prime}{}_{species\,2} \qquad (1)$$

Given that the formal potential of the reporter reaction is constant on all electrodes in an array, a difference in the driving potential at the onset of ECL coupling for two electrodes equates to their difference in HER onset potential. **Figure 2e** shows false color plot corresponding to the Pt deposition mapped in **Figure 2f**. Note that electrodes at the center of the injection site exhibit the lowest HER onset potentials, but these values quickly increase for electrodes located further away from this position. Also, the same tailing which was observed in the EDS map covers an even greater area in this plot, indicating that imaging the catalytic activity via this scheme is even more sensitive than EDS for detecting the presence of Pt.

After mapping the HER performance across the deposition site, SEM was used to examine the metal coverage of individual electrodes. Due to the geometric arrangement of the arrayed electrodes and the excellent contrast between the deposited Pt and underlying carbon, imaging of specific electrodes exhibiting an ECL signal of interest was relatively straightforward (see designated electrodes in **Figure 2e**) and yielded a positive correlation between the catalytic performance of individual electrodes and the coverage of Pt on their surfaces (**Figures 2a-d**). Such a relationship is to be expected given the higher

local metal ion concentration present about the pipette orifice during injection which would result in greater Pt surface areas on the nearby electrodes and correspondingly elevated catalytic current levels. These results demonstrate the efficacy of this gradient electrodeposition method coupled with bipolar coupling and ECL imaging as a high-throughput platform for generating and screening large pools of compositionally gradient electrocatalyst samples.

Screening Electrocatalyst Composition with Au-Modified Bipolar UME Arrays. To further expand the applications of this array-based catalysis imaging scheme toward the investigation of more complex interfacial and bimetallic catalytic systems, the fabrication scheme for the carbon bipolar UME arrays was updated to incorporate a metal coating on the electrodes' detecting poles. Au was selected as the modifying material due to its ease of patterning via wet etching. Briefly, 200 nm of Au was sputtered over the surface of the devices immediately following pyrolysis, after which the Au-coated electrodes were insulated in Parylene C and exposed via plasma etching. The arrays were annealed in a tube furnace at 400°C under a N_2 flow which typically resulted in delamination of the devices from the substrate. Each released array was then epoxied to a well on its upper surface, after which the lower surface was immersed in Au etchant to remove the metal connecting the individual electrodes (fabrication process outlined in **Scheme S1**). This same process may be readily extended to facilitate modification of a bipolar UME array with any other metal which can be wet etched. Note that the reporting poles of these Au-coated arrays still consist of bare carbon to ensure that the kinetics of the ECL reporter reaction remain unchanged relative to the original unmodified design. The resulting arrays appeared extremely uniform under SEM characterization (see **Figure 3a,b**) and revealed virtually identical optical responses from all electrodes when used to couple HER in acidic solution to anodic ECL (mean onset driving potential of 1155.6 mV and standard deviation of 15.6 mV, see **Figure 3c**).

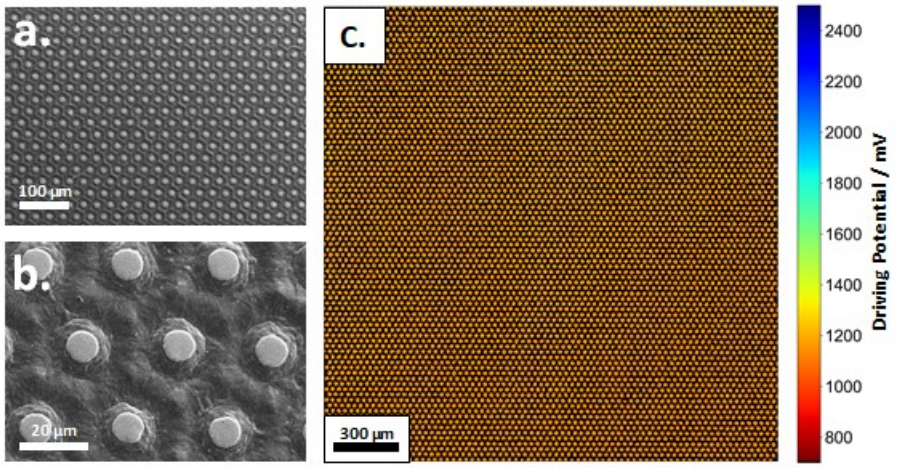

Figure 3. (a,b) SEM images of Au-coated bipolar UME array. (c) False color plot of HER onset driving potentials of Au-coated bipolar UME array in 100 mM $HClO_4$ 100 mM NaCl coupled to anodic ECL.

A metal/metal hydroxide electrocatalyst was selected for investigation to demonstrate the utility of these Au-coated arrays in interfacial catalyst screening and compositional optimization studies. This electrocatalytic scheme was originally introduced to enhance the HER activity of Pt in alkaline solution by decorating the metal surface with $Ni(OH)_2$ islands to encourage adsorption of OH^- on the metal hydroxide clusters and H^+ on the Pt surface, thereby promoting water dissociation which is the rate determining step of the HER in basic solution.[57] Modification with metal hydroxides has since been demonstrated to similarly improve the HER performance of other transition metal electrocatalysts (such as Au, Ag, Cu, Ru etc.) which underperform in basic solution due to slow water dissociation kinetics.[58–60] However, oversaturation of the electrode surface results in adverse effects to HER activity due to the poor conductivity of $Ni(OH)_2$[61–63] and obstruction of active sites on the transition metal surface necessary for H adsorption.[64–66] Such a prediction therefore implies the existence of an optimum degree of metal hydroxide surface coverage for maximum electrocatalyst performance; this proposed relationship will be further explored here.

An initial experiment to confirm the predicted link between these two parameters was carried out using a 25 µm Au UME in which the unbiased electrode was immersed in a $NiCl_2$ solution for intervals ranging from 10 s to 5 min to modify the surface with increasing amounts of $Ni(OH)_2$ as has been

described and characterized elsewhere.[58] The UME was then rinsed with DI water and transferred to 100 mM KOH where its potential was scanned from 0 to -2 V vs. Ag/AgCl and the resulting current response recorded. Note from **Figure 4a** that immersion times of 10 s and 1 min in the $NiCl_2$ solution result in corresponding decreases in HER onset potential relative to the unmodified Au surface; however, an immersion time of 5 min displays a drastic negative shift in current onset with the observed response reduced to almost zero over the displayed potential range. This reduction in activity is consistent with blockage of the electrode surface by the metal hydroxide despite the synergistic enhancement to alkaline HER activity which was brought on by initial modification.

To further verify this relationship in a more parallelized fashion, a gradient of $Ni(OH)_2$ was generated across the surface of an Au-coated array by first employing a micropipette to dispense a concentrated $NiCl_2$ solution at the array surface which was contacting a Hg drop biased at a reducing potential; pipette diameter, distance from the array surface, injection pressure/time, and bulk electrolyte concentration were unchanged from the Pt deposition conditions. The electrolyte solution was then replaced with 100 mM KOH and the applied potential scanned[67,68] between 0.1 and 0.5 V vs. Ag/AgCl at 5 mV/s to oxidize the deposited Ni to $Ni(OH)_2$; potential cycling was ceased after 25 cycles when the anodic current was observed to be zero. **Figure S2e** shows a representative EDS map of a $Ni(OH)_2$ gradient generated on an Au-coated array which exhibits a clear radial decrease in Ni signal about the location of the micropipette injection. Additionally, SEM micrographs of selected electrodes from the EDS map confirm this trend in deposited $Ni(OH)_2$, with coverage ranging from almost total encapsulation of the electrode surfaces near the center of the spot to virtually nothing at the periphery (**Figure S2a-d**). Note, however, that the nature of the SEM/EDS sample prep (*i.e.*, affixation to a Si substrate with conductive epoxy followed by carbon coating) prevented further use of arrays characterized in this fashion. Subsequent experiments were therefore carried out with identically prepared devices.

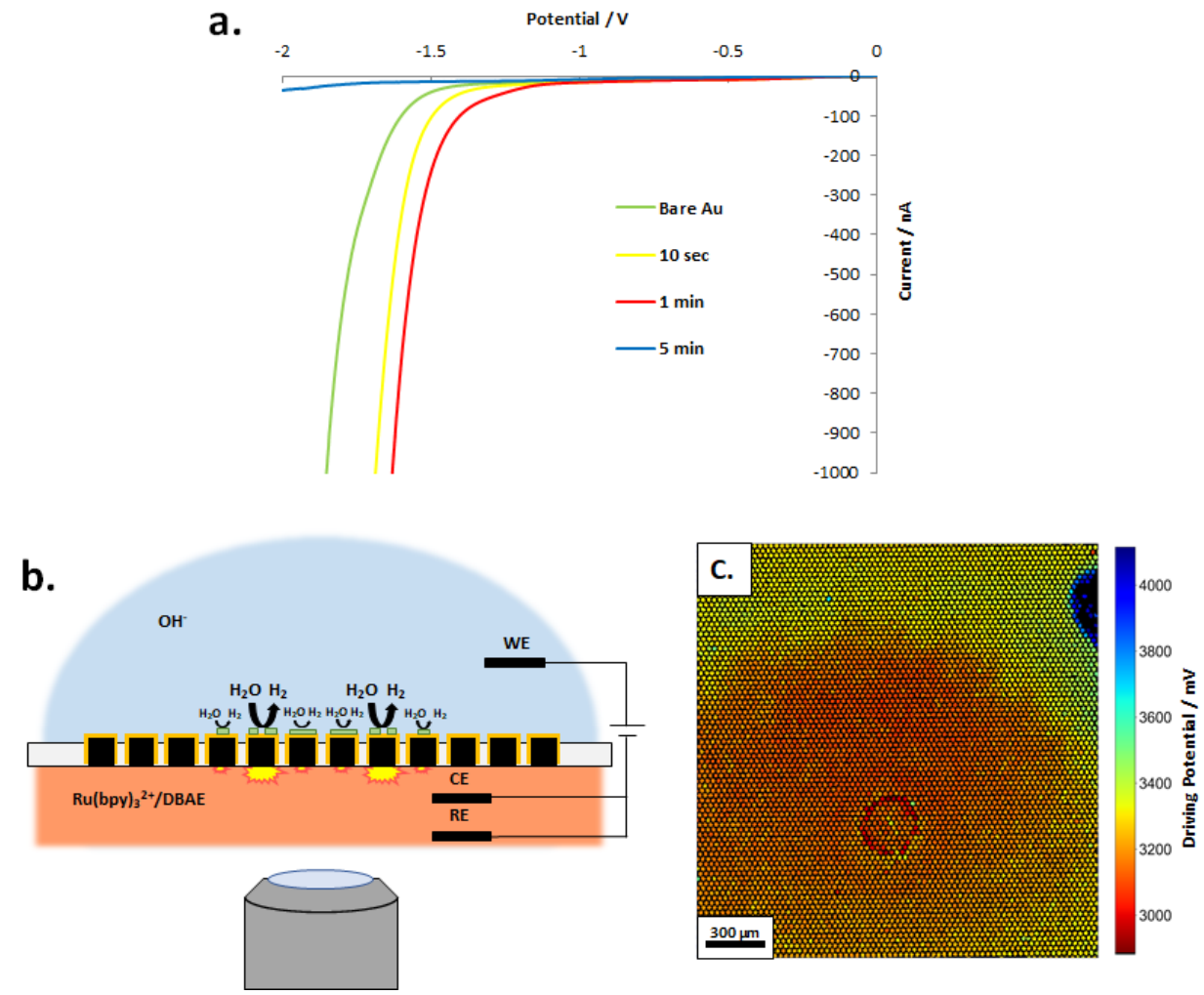

Figure 4. (a) Linear sweep voltammograms for a 25 µm Au UME with varying immersion times in 1 M $NiCl_2$ 100 mM NaCl pH 3.6. (b) Diagram of a screening experiment with a gradient of $Ni(OH)_2$ on an Au-coated bipolar UME array. (c) False color plot of HER onset driving potentials of a $Ni(OH)_2$-modified Au-coated bipolar UME array in 100 mM KOH 100 coupled to anodic ECL.

After $Ni(OH)_2$ deposition, the HER activity of the array in 100 mM KOH was imaged via coupling to anodic ECL using a driving potential scan of 0 to 4 V vs. Ag/AgCl (scheme shown in **Figure 4b** and raw data in **Movie S2**). The resulting activity false color plot (**Figure 4c**) for the center of the $Ni(OH)_2$ gradient exhibits a ~300 mV decrease in the magnitude of HER onset potential relative to bare Au for electrodes located in a narrow ~250 µm diameter ring with less pronounced enhancements to activity being observed outside this region. This increase in activity is consistent with the potential shift observed for the voltammogram exhibiting the highest HER activity in **Figure 4a** (1 min immersion

time). The presence of this peak in activity indicates that optimal modification of the Au surface was achieved at this point in the radial $Ni(OH)_2$ gradient about the deposition site, with higher or lower coverage outside this region resulting in diminished catalytic performance (the zone exhibiting extremely low activity in the upper right of the plot is due to the application of epoxy which was used to seal a defect in the array). These results further confirm the predicted nature of the relationship between alkaline HER performance and the surface coverage of the modifying metal hydroxide on a transition metal surface and also demonstrate the utility of this gradient deposition technique and array-based screening platform in exploring the effects of compositional variation on electrocatalytic activity.

Conclusions

In summary, we have demonstrated the use of massive bipolar UME arrays in conjunction with ECL imaging as a high-throughput platform capable of simultaneously screening several thousand electrocatalyst compositions. Additionally, we have introduced a complementary technique for electrodeposition of a radial gradient of catalytic metal on the surface of these arrays for the purpose of rapidly generating large quantities of compositionally varied electrocatalyst samples. Lastly, we have utilized both of these methods in conjunction with a new process for uniform metal modification of the aforementioned arrays to investigate the impact of varied $Ni(OH)_2$ coverage on the HER activity of an Au surface in alkaline solution, with the catalytic performance of the modified Au being confirmed to exhibit a peak-shaped dependence on increasing $Ni(OH)_2$ coverage. Future work will focus on further expanding this platform to enable the screening of metal alloys by incorporating additional micropipettes for the purpose of simultaneously delivering multiple metal salt solutions to the array surface during the gradient electrodeposition process; X-ray photoelectron spectroscopy (XPS) measurements of catalyst compositions will also be the focus of subsequent studies.

Acknowledgements

This research was supported by the National Science Foundation (CHE-1904426). Part of this work was conducted at the Molecular Analysis Facility, a National Nanotechnology Coordinated Infrastructure site at the University of Washington which is supported in part by the National Science Foundation (grant ECC-1542101), the University of Washington, the Molecular Engineering & Sciences Institute, the Clean Energy Institute, and the National Institutes of Health. Part of this work was also conducted at the Washington Nanofabrication Facility / Molecular Analysis Facility, a National Nanotechnology Coordinated Infrastructure (NNCI) site at the University of Washington, which is supported in part by funds from the National Science Foundation (awards NNCI-1542101, 1337840 and 0335765), the National Institutes of Health, the Molecular Engineering & Sciences Institute, the Clean Energy Institute, the Washington Research Foundation, the M. J. Murdock Charitable Trust, Altatech, ClassOne Technology, GCE Market, Google and SPTS.

References

(1) Wang, Y.-J.; Zhao, N.; Fang, B.; Li, H.; Bi, X. T.; Wang, H. Carbon-Supported Pt-Based Alloy Electrocatalysts for the Oxygen Reduction Reaction in Polymer Electrolyte Membrane Fuel Cells: Particle Size, Shape, and Composition Manipulation and Their Impact to Activity. *Chem. Rev.* **2015**, *115*, 3433–3467.

(2) Lenne, Q.; Leroux, Y. R.; Lagrost, C. Surface Modification for Promoting Durable, Efficient, and Selective Electrocatalysts. *ChemElectroChem* **2020**, *7*, 2345–2363.

(3) Wang, C.; Markovic, N. M.; Stamenkovic, V. R. Advanced Platinum Alloy Electrocatalysts for the Oxygen Reduction Reaction. *ACS Catal.* **2012**, *2*, 891–898.

(4) Gamler, J. T. L.; Ashberry, H. M.; Skrabalak, S. E.; Koczkur, K. M. Random Alloyed versus Intermetallic Nanoparticles: A Comparison of Electrocatalytic Performance. *Adv. Mater.* **2018**, *30*, 1801563.

(5) Smotkin, E. S.; Díaz-Morales, R. R. New Electrocatalysts by Combinatorial Methods. *Annu. Rev. Mater. Res.* **2003**, *33*, 557–579.

(6) Jeon, M. K.; Lee, C. H.; Park, G. I.; Kang, K. H. Combinatorial Search for Oxygen Reduction Reaction Electrocatalysts: A Review. *J. Power Sources* **2012**, *216*, 400–408.

(7) Antolini, E. Evaluation of the Optimum Composition of Low-Temperature Fuel Cell Electrocatalysts for Methanol Oxidation by Combinatorial Screening. *ACS Comb. Sci.* **2017**, *19*, 47–54.

(8) Guerin, S.; Hayden, B. E.; Lee, C. E.; Mormiche, C.; Owen, J. R.; Russell, A. E.; Theobald, B.; Thompsett, D. Combinatorial Electrochemical Screening of Fuel Cell Electrocatalysts. *J. Comb. Chem.* **2004**, *6*, 149–158.

(9) Smotkin, E. S.; Jiang, J.; Nayar, A.; Liu, R. High-Throughput Screening of Fuel Cell Electrocatalysts. *Appl. Surf. Sci.* **2006**, *252*, 2573–2579.

(10) Reddington, E. Combinatorial Electrochemistry: A Highly Parallel, Optical Screening Method for Discovery of Better Electrocatalysts. *Science* **1998**, *280*, 1735–1737.

(11) Jayaraman, S.; Hillier, A. C. Screening the Reactivity of $Pt_x Ru_y$ and $Pt_x Ru_y Mo_z$ Catalysts toward the Hydrogen Oxidation Reaction with the Scanning Electrochemical Microscope. *J. Phys. Chem. B* **2003**, *107*, 5221–5230.

(12) Fernández, J. L.; White, J. M.; Sun, Y.; Tang, W.; Henkelman, G.; Bard, A. J. Characterization and Theory of Electrocatalysts Based on Scanning Electrochemical Microscopy Screening Methods. *Langmuir* **2006**, *22*, 10426–10431.

(13) Spong, A. D.; Vitins, G.; Guerin, S.; Hayden, B. E.; Russell, A. E.; Owen, J. R. Combinatorial Arrays and Parallel Screening for Positive Electrode Discovery. *J. Power Sources* **2003**, *119–121*, 778–783.

(14) Fernández, J. L.; Walsh, D. A.; Bard, A. J. Thermodynamic Guidelines for the Design of Bimetallic Catalysts for Oxygen Electroreduction and Rapid Screening by Scanning Electrochemical Microscopy. M−Co (M: Pd, Ag, Au). *J. Am. Chem. Soc.* **2005**, *127*, 357–365.

(15) Latyshev, V.; Vorobiov, S.; Shylenko, O.; Komanicky, V. Fabrication of Combinatorial Material Libraries by Flow Cell Electrodeposition Technique. *Mater. Lett.* **2020**, *281*, 128594.

(16) Guerin, S.; Hayden, B. E. Physical Vapor Deposition Method for the High-Throughput Synthesis of Solid-State Material Libraries. *J. Comb. Chem.* **2006**, *8*, 66–73.

(17) Prochaska, M.; Jin, J.; Rochefort, D.; Zhuang, L.; DiSalvo, F. J.; Abruña, H. D.; van Dover, R. B. High Throughput Screening of Electrocatalysts for Fuel Cell Applications. *Rev. Sci. Instrum.* **2006**, *77*, 054104.

(18) Guerin, S.; Hayden, B. E.; Lee, C. E.; Mormiche, C.; Russell, A. E. High-Throughput Synthesis and Screening of Ternary Metal Alloys for Electrocatalysis. *J. Phys. Chem. B* **2006**, *110*, 14355–14362.

(19) Latyshev, V.; Vorobiov, S.; Shylenko, O.; Komanicky, V. Screening of Electrocatalysts for Hydrogen Evolution Reaction Using Bipolar Electrodes Fabricated by Composition Gradient Magnetron Sputtering. *J. Electroanal. Chem.* **2019**, *854*, 113562.

(20) Yang, Y.; Chen, G.; Zeng, R.; Villarino, A. M.; DiSalvo, F. J.; van Dover, R. B.; Abruña, H. D. Combinatorial Studies of Palladium-Based Oxygen Reduction Electrocatalysts for Alkaline Fuel Cells. *J. Am. Chem. Soc.* **2020**, *142*, 3980–3988.

(21) Termebaf, H.; Shayan, M.; Kiani, A. Two-Step Bipolar Electrochemistry: Generation of Composition Gradient and Visual Screening of Electrocatalytic Activity. *Langmuir* **2015**, *31*, 13238–13246.

(22) Minguzzi, A.; Alpuche-Aviles, M. A.; López, J. R.; Rondinini, S.; Bard, A. J. Screening of Oxygen Evolution Electrocatalysts by Scanning Electrochemical Microscopy Using a Shielded Tip Approach. *Anal. Chem.* **2008**, *80*, 4055–4064.

(23) Minguzzi, A.; Battistel, D.; Rodríguez-López, J.; Vertova, A.; Rondinini, S.; Bard, A. J.; Daniele, S. Rapid Characterization of Oxygen-Evolving Electrocatalyst Spot Arrays by the Substrate Generation/Tip Collection Mode of Scanning Electrochemical Microscopy with Decreased O_2 Diffusion Layer Overlap. *J. Phys. Chem. C* **2015**, *119*, 2941–2947.

(24) Li, W.; Fan, F.-R. F.; Bard, A. J. The Application of Scanning Electrochemical Microscopy to the Discovery of Pd–W Electrocatalysts for the Oxygen Reduction Reaction That Demonstrate High Activity, Stability, and Methanol Tolerance. *J. Solid State Electrochem.* **2012**, *16*, 2563–2568.

(25) Walsh, D. A.; Fernández, J. L.; Bard, A. J. Rapid Screening of Bimetallic Electrocatalysts for Oxygen Reduction in Acidic Media by Scanning Electrochemical Microscopy. *J. Electrochem. Soc.* **2006**, *153*, E99.

(26) Jung, C.; Sánchez-Sánchez, C. M.; Lin, C.-L.; Rodríguez-López, J.; Bard, A. J. Electrocatalytic Activity of Pd−Co Bimetallic Mixtures for Formic Acid Oxidation Studied by Scanning Electrochemical Microscopy. *Anal. Chem.* **2009**, *81*, 7003–7008.

(27) Lee, K. R.; Jeon, M. K.; Woo, S. I. Composition Optimization of PtRuM/C (M=Fe and Mo) Catalysts for Methanol Electro-Oxidation via Combinatorial Method. *Appl. Catal. B Environ.* **2009**, *91*, 428–433.

(28) Lee, K. R.; Jung, Y.; Woo, S. I. Combinatorial Screening of Highly Active Pd Binary Catalysts for Electrochemical Oxygen Reduction. *ACS Comb. Sci.* **2012**, *14*, 10–16.

(29) Schuppert, A. K.; Topalov, A. A.; Katsounaros, I.; Klemm, S. O.; Mayrhofer, K. J. J. A Scanning Flow Cell System for Fully Automated Screening of Electrocatalyst Materials. *J. Electrochem. Soc.* **2012**, *159*, F670.

(30) Lai, Y.; Jones, R. J. R.; Wang, Y.; Zhou, L.; Gregoire, J. M. Scanning Electrochemical Flow Cell with Online Mass Spectroscopy for Accelerated Screening of Carbon Dioxide Reduction Electrocatalysts. *ACS Comb. Sci.* **2019**, *21*, 692–704.

(31) Woodhouse, M.; Parkinson, B. A. Combinatorial Discovery and Optimization of a Complex Oxide with Water Photoelectrolysis Activity. *Chem. Mater.* **2008**, *20*, 2495–2502.

(32) Sullivan, M. G.; Utomo, H.; Fagan, P. J.; Ward, M. D. Automated Electrochemical Analysis with Combinatorial Electrode Arrays. *Anal. Chem.* **1999**, *71*, 4369–4375.

(33) Strasser, P.; Fan, Q.; Devenney, M.; Weinberg, W. H.; Liu, P.; Nørskov, J. K. High Throughput Experimental and Theoretical Predictive Screening of Materials − A Comparative Study of Search Strategies for New Fuel Cell Anode Catalysts. *J. Phys. Chem. B* **2003**, *107*, 11013–11021.

(34) Dang, T.; Ramsaran, R.; Roy, S.; Froehlich, J.; Wang, J.; Kubiak, C. P. Design of a High Throughput 25-Well Parallel Electrolyzer for the Accelerated Discovery of CO2 Reduction Catalysts via a Combinatorial Approach. *Electroanalysis* **2011**, *23*, 2335–2342.

(35) Zhang, Y.; McGinn, P. J. Combinatorial Screening for Methanol Oxidation Catalysts in Alloys of Pt, Cr, Co and V. *J. Power Sources* **2012**, *206*, 29–36.

(36) Brace, K. M.; Hayden, B. E.; Russell, A. E.; Owen, J. R. A Parallel Optical Screen for the Rapid Combinatorial Electrochromic Analysis of Electrochemical Materials. *Adv. Mater.* **2006**, *18*, 3253–3257.

(37) Jaramillo, T. F.; Ivanovskaya, A.; McFarland, E. W. High-Throughput Screening System for Catalytic Hydrogen-Producing Materials. *J. Comb. Chem.* **2002**, *4*, 17–22.

(38) Xiang, C.; Suram, S. K.; Haber, J. A.; Guevarra, D. W.; Soedarmadji, E.; Jin, J.; Gregoire, J. M. High-Throughput Bubble Screening Method for Combinatorial Discovery of Electrocatalysts for Water Splitting. *ACS Comb. Sci.* **2014**, *16*, 47–52.

(39) Fosdick, S. E.; Crooks, R. M. Bipolar Electrodes for Rapid Screening of Electrocatalysts. *J. Am. Chem. Soc.* **2012**, *134*, 863–866.

(40) Fosdick, S. E.; Berglund, S. P.; Mullins, C. B.; Crooks, R. M. Parallel Screening of Electrocatalyst Candidates Using Bipolar Electrochemistry. *Anal. Chem.* **2013**, *85*, 2493–2499.

(41) Fosdick, S. E.; Berglund, S. P.; Mullins, C. B.; Crooks, R. M. Evaluating Electrocatalysts for the Hydrogen Evolution Reaction Using Bipolar Electrode Arrays: Bi- and Trimetallic Combinations of Co, Fe, Ni, Mo, and W. *ACS Catal.* **2014**, *4*, 1332–1339.

(42) Chow, K.-F.; Mavré, F.; Crooks, R. M. Wireless Electrochemical DNA Microarray Sensor. *J. Am. Chem. Soc.* **2008**, *130*, 7544–7545.

(43) Chow, K.-F.; Mavré, F.; Crooks, J. A.; Chang, B.-Y.; Crooks, R. M. A Large-Scale, Wireless Electrochemical Bipolar Electrode Microarray. *J. Am. Chem. Soc.* **2009**, *131*, 8364–8365.

(44) Mavré, F.; Chow, K.-F.; Sheridan, E.; Chang, B.-Y.; Crooks, J. A.; Crooks, R. M. A Theoretical and Experimental Framework for Understanding Electrogenerated Chemiluminescence (ECL) Emission at Bipolar Electrodes. *Anal. Chem.* **2009**, *81*, 6218–6225.

(45) Fosdick, S. E.; Knust, K. N.; Scida, K.; Crooks, R. M. Bipolar Electrochemistry. *Angew. Chem. Int. Ed.* **2013**, *52*, 10438–10456.

(46) Bouffier, L.; Zigah, D.; Sojic, N.; Kuhn, A. Bipolar (Bio)Electroanalysis. *Annu. Rev. Anal. Chem.* **2021**, *14*, 65–86.

(47) Cox, J. T.; Guerrette, J. P.; Zhang, B. Steady-State Voltammetry of a Microelectrode in a Closed Bipolar Cell. *Anal. Chem.* **2012**, *84*, 8797–8804.

(48) Guerrette, J. P.; Oja, S. M.; Zhang, B. Coupled Electrochemical Reactions at Bipolar Microelectrodes and Nanoelectrodes. *Anal. Chem.* **2012**, *84*, 1609–1616.

(49) Lin, X.; Zheng, L.; Gao, G.; Chi, Y.; Chen, G. Electrochemiluminescence Imaging-Based High-Throughput Screening Platform for Electrocatalysts Used in Fuel Cells. *Anal. Chem.* **2012**, *84*, 7700–7707.

(50) Zhang, J.-D.; Hao, N.; Lu, L.; Yun, S.; Zhu, X.-F.; Hong, K.; Feng, L.-D. High-Efficient Preparation and Screening of Electrocatalysts Using a Closed Bipolar Electrode Array System. *J. Electroanal. Chem.* **2019**, *832*, 1–6.

(51) Anderson, T. J.; Defnet, P. A.; Zhang, B. Electrochemiluminescence (ECL)-Based Electrochemical Imaging Using a Massive Array of Bipolar Ultramicroelectrodes. *Anal. Chem.* **2020**, *92*, 6748–6755.

(52) Guerrette, J. P.; Percival, S. J.; Zhang, B. Fluorescence Coupling for Direct Imaging of Electrocatalytic Heterogeneity. *J. Am. Chem. Soc.* **2013**, *135*, 855–861.

(53) Defnet, P. A.; Zhang, B. Detection of Transient Nanoparticle Collision Events Using Electrochemiluminescence on a Closed Bipolar Microelectrode. *ChemElectroChem* **2020**, *7*, 252–259.

(54) V. Macpherson, J.; A. Beeston, M.; R. Unwin, P. Imaging Local Mass-Transfer Rates within an Impinging Jet and Studies of Fast Heterogeneous Electron-Transfer Kinetics Using the Microjet Electrode. *J. Chem. Soc. Faraday Trans.* **1995**, *91*, 899–904.

(55) Macpherson, J. V.; Simjee, N.; Unwin, P. R. Hydrodynamic Ultramicroelectrodes: Kinetic and Analytical Applications. *Electrochimica Acta* **2001**, *47*, 29–45.

(56) Bitziou, E.; Rudd, N. C.; Edwards, M. A.; Unwin, P. R. Visualization and Modeling of the Hydrodynamics of an Impinging Microjet. *Anal. Chem.* **2006**, *78*, 1435–1443.

(57) Subbaraman, R.; Tripkovic, D.; Strmcnik, D.; Chang, K.-C.; Uchimura, M.; Paulikas, A. P.; Stamenkovic, V.; Markovic, N. M. Enhancing Hydrogen Evolution Activity in Water Splitting by Tailoring Li+-Ni(OH)2-Pt Interfaces. *Science* **2011**, *334*, 1256–1260.

(58) Danilovic, N.; Subbaraman, R.; Strmcnik, D.; Chang, K.-C.; Paulikas, A. P.; Stamenkovic, V. R.; Markovic, N. M. Enhancing the Alkaline Hydrogen Evolution Reaction Activity through the Bifunctionality of $Ni(OH)_2$ /Metal Catalysts. *Angew. Chem.* **2012**, *124*, 12663–12666.

(59) Chen, Z.; Duan, X.; Wei, W.; Wang, S.; Ni, B.-J. Recent Advances in Transition Metal-Based Electrocatalysts for Alkaline Hydrogen Evolution. *J. Mater. Chem. A* **2019**, *7*, 14971–15005.

(60) Zhu, Y.; Lin, Q.; Zhong, Y.; Tahini, H. A.; Shao, Z.; Wang, H. Metal Oxide-Based Materials as an Emerging Family of Hydrogen Evolution Electrocatalysts. *Energy Environ. Sci.* **2020**, *13*, 3361–3392.

(61) Wu, H.; Zhu, T.; Lu, X.; Wei Ho, G. High-Efficient Electrocatalysts by Unconventional Acid-Etching for Overall Water Splitting. *J. Mater. Chem. A* **2017**, *5*, 24153–24158.

(62) Xie, L.; Ren, X.; Liu, Q.; Cui, G.; Ge, R.; M. Asiri, A.; Sun, X.; Zhang, Q.; Chen, L. A Ni(OH) 2 –PtO 2 Hybrid Nanosheet Array with Ultralow Pt Loading toward Efficient and Durable Alkaline Hydrogen Evolution. *J. Mater. Chem. A* **2018**, *6*, 1967–1970.

(63) Liu, Q.; Yan, Z.; Gao, J.; Wang, E.; Sun, G. Optimizing Platinum Location on Nickel Hydroxide Nanosheets to Accelerate the Hydrogen Evolution Reaction. *ACS Appl. Mater. Interfaces* **2020**, *12*, 24683–24692.

(64) Wang, L.; Lin, C.; Huang, D.; Chen, J.; Jiang, L.; Wang, M.; Chi, L.; Shi, L.; Jin, J. Optimizing the Volmer Step by Single-Layer Nickel Hydroxide Nanosheets in Hydrogen Evolution Reaction of Platinum. *ACS Catal.* **2015**, *5*, 3801–3806.

(65) Yu, X.; Zhao, J.; Zheng, L.-R.; Tong, Y.; Zhang, M.; Xu, G.; Li, C.; Ma, J.; Shi, G. Hydrogen Evolution Reaction in Alkaline Media: Alpha- or Beta-Nickel Hydroxide on the Surface of Platinum? *ACS Energy Lett.* **2018**, *3*, 237–244.

(66) Wang, G.; Parrondo, J.; He, C.; Li, Y.; Ramani, V. Pt/C/Ni(OH)2 Bi-Functional Electrocatalyst for Enhanced Hydrogen Evolution Reaction Activity under Alkaline Conditions. *J. Electrochem. Soc.* **2017**, *164*, F1307.

(67) E, S. P.; Liu, D.; Lazenby, R. A.; Sloan, J.; Vidotti, M.; Unwin, P. R.; Macpherson, J. V. Electrodeposition of Nickel Hydroxide Nanoparticles on Carbon Nanotube Electrodes: Correlation of Particle Crystallography with Electrocatalytic Properties. *J. Phys. Chem. C* **2016**, *120*, 16059–16068.

(68) Tucceri, R. An Electrochemical Study of the Nickel Hydroxide-Gold Modified Electrode Employing the Surface Resistance Technique. *J. Electroanal. Chem.* **2016**, *774*, 95–101.